Sensors and Actuators B 222 (2016) 893–903

Contents lists available at ScienceDirect

Sensors and Actuators B: Chemical

journal homepage: www.elsevier.com/locate/snb

Preparation of Ag nanoparticles-SnO_2 nanoparticles-reduced graphene oxide hybrids and their application for detection of NO_2 at room temperature

Ziying Wang[a,b], Yong Zhang[a], Sen Liu[a,**], Tong Zhang[a,b,*]

[a] State Key Laboratory of Integrated Optoelectronics, College of Electronic Science and Engineering, Jilin University, Changchun, PR China
[b] State Key Laboratory of Transducer Technology, Chinese Academy of Sciences, PR China

ARTICLE INFO

Article history:
Received 3 July 2015
Received in revised form 31 August 2015
Accepted 6 September 2015
Available online 8 September 2015

Keywords:
Reduced graphene oxide
Tin dioxide nanoparticle
Silver nanoparticle
Nitrogen dioxide
Room temperature

ABSTRACT

A novel NO_2 gas sensor has been constructed using Ag nanoparticles-SnO_2 nanoparticles-reduced graphene oxide (AgNPs-SnO_2-rGO) hybrids as sensing materials. AgNPs-SnO_2-rGO hybrids were prepared by a two-step wet-chemical method. Firstly, SnO_2-rGO hybrids were synthesized by hydrothermal treatment of aqueous dispersion of GO in the presence of $SnCl_4$. Then, AgNPs-SnO_2-rGO hybrids were obtained by in situ reduction of $AgNO_3$ on the surface of SnO_2-rGO hybrids. The combined characterizations of UV–vis spectroscopy, X-ray diffraction (XRD), energy-dispersive X-ray spectrometer (EDX), elemental mapping, X-ray photoelectron spectroscopy (XPS), transmission electron microscopy (TEM) and Raman spectra were used to investigate the structure of AgNPs-SnO_2-rGO hybrids. Most importantly, the sensor based on AgNPs-SnO_2-rGO hybrids exhibits good sensing performance for NO_2 sensing operating at room temperature. For example, the response time and recovery time of the sensor based on AgNPs-SnO_2-rGO hybrids for 5 ppm NO_2 are 49 s and 339 s, which are much shorter than that of SnO_2-rGO hybrids (415 s and 740 s), indicating that the sensing performances for NO_2 sensing at room temperature have been tremendously enhanced by introduction of AgNPs into SnO_2-rGO hybrids.

1. Introduction

It is well known that nitrogen dioxide (NO_2) is a common toxic and harmful gas, and NO_2 primarily comes from burning fuel at high temperature and exhaust of motor vehicle. The increase levels of NO_2 in cities cause dramatic environmental pollution as well as severe damages on human respiratory tract [1,2]. The detection of NO_2 is thus of great importance in both environmental protection and human health. Therefore, the development of high performance detection techniques for detection of NO_2 has important scientific significance and application value.

Up to now, numerous techniques have been successfully developed for detection of NO_2, such as metal oxide semiconductor-based gas sensors, solid electrolyte-based gas sensors, optic fiber and surface acoustic wave (SAW) devices [3–6]. Among them, metal oxide semiconductor-type NO_2 gas sensors have attracted much interest, due to their good sensing performances including high response, fast response and recovery rate. The good sensing performances could be attributed to unique properties of metal oxides, such as high surface-to-volume ratio, tunable surface defects, abundant active sites and so on. Indeed, the typical metal oxides including WO_3, ZnO, SnO_2, In_2O_3 have been successfully used for fabrication of NO_2 gas sensors [7–10]. However, these sensors are always operated at high temperature, resulting in high power consumption and difficulty in integration. Therefore, development of NO_2 sensors operating at room temperature has important practical significance.

Graphene is a typical two-dimensional sheet of sp^2-hybridized carbon atoms nanostructure, which exhibits excellent chemical and physical properties, such as high specific surface area, high thermal stability, good mechanical strength, good electronic conductivity, carrier mobility at room temperature, etc. [11–13]. Hence, graphene has been considered as a promising sensing material for gas detection at room temperature [14,15]. Although various NO_2 sensors have been successfully constructed by using reduced graphene oxide (rGO)-based materials as sensing materials, the relatively poor performances such as low response, long response time and recovery time should be further improved. It is well known that

* Corresponding author at: State Key Laboratory of Integrated Optoelectronics, College of Electronic Science and Engineering, Jilin University, Changchun, PR China.
** Corresponding author.
E-mail addresses: liusen@jlu.edu.cn (S. Liu), zhangtong@jlu.edu.cn (T. Zhang).

http://dx.doi.org/10.1016/j.snb.2015.09.027
0925-4005/

the response of rGO-based gas sensors is attributed to the interaction between NO_2 molecule and active sites (mainly defect) in rGO [16]. Thus, the response (or sensitivity) is subjected to the amount of defects in rGO. Unfortunately, the relatively low content of defects in pure rGO results in poor response (or sensitivity) for NO_2 sensing, which have been further confirmed by Huang's report that the porous rGO exhibits higher response to NO_2 than that of conventional rGO [17]. The long response time and recovery time are related to interaction between NO_2 molecules and high-energy binding sites (such as vacancies, defects, and oxygen functional groups), and the thermal energy of rGO is usually insufficient to overcome the activation energy for desorption, leading to slow response and recovery rate [18].

To overcome these problems, modification of rGO-based materials with metal oxides has been proven as an effective method for enhancing NO_2 sensing performances. During the past few years, different n-type metal oxides (SnO_2, ZnO, WO_3) and p-type metal oxides (Co_3O_4, Cu_2O) have been successfully used for modification of rGO, which exhibit better sensing performances for detection of NO_2 at room temperature than that of pure rGO [19–22]. The modification of rGO with metal oxides could enhance sensing performances, which may be attributed to the following three important factors: (i) the tailoring of the surface active sites [23], (ii) increasing the specific surface area [24], and (ii) the heterojunction formed at the interface between n-type metal oxide (such as SnO_2, ZnO, WO_3) and p-type rGO [24,25].

Among all the rGO-metal oxide hybrids, SnO_2 modified rGO nanocomposites have attracted much attention because SnO_2 materials are promising materials for detection of gases at relatively high operating temperature. For example, Lee et al. have prepared SnO_2 nanofibers loading rGO nanosheets by electrospinning method for detection of NO_2 at 200 °C [25]; Marichy et al. have fabricated SnO_2-rGO heterostructures for detection of NO_2 at 150 °C [26]; Neri et al. have examined sensing behavior of SnO_2/rGO nanocomposites for detection of NO_2 at 200 °C [27]. Although good sensing performances are observed by addition of SnO_2 into rGO matrix, relatively high operating temperature is required for detection of NO_2. Alternatively, the high carrier mobility ensures that rGO also a good candidate for fabrication of gas sensor operating at room temperature. For instance, Mao et al. have reported that the sensor based on SnO_2 nanocrystals-rGO shows a low detection limit (1 ppm) with the sensitivity of 1.11 to NO_2 at room temperature [28]; Cui et al. have synthesized indium-doped SnO_2 nanoparticles on rGO for NO_2 detection at room temperature with low concentration detection (1 ppm) [29]; Liu et al. and Li et al. have developed novel NO_2 sensors using 3D graphene supported SnO_2 as sensing materials for detection of NO_2 at room temperature [30,31]. It is obviously seen that these efforts have been devoted to enhancing the sensing properties of rGO-based materials by introduction of SnO_2 materials. However, the sensors based on SnO_2-rGO still have more or less disadvantages, such as low sensitivity, long recovery times, high operating temperature, etc.

Recently, we have fabricated NO_2 sensors using SnO_2-rGO hybrids as sensing materials. Although the sensors exhibit better sensing performances than that of rGO, the sensors are also required heating (operated at 50 °C) for detection of gases [32]. In spite of these reports, developing rGO-based high-performance gas sensors for detection of NO_2 at room temperature is indeed necessary. More recently, we have developed a new strategy for improvement of sensing performances toward NO_2 detection by introduction of multiwalled carbon nanotubes (MWCNTs) into the SnO_2-rGO hybrids, paving the pathway for enhancing sensing performances of rGO-based NO_2 sensors by preparation of ternary rGO-based hybrids [33].

On the other hand, introduction of noble metals into metal oxide-based sensing materials has been widely used for the improvement of gas sensing performances at high operating temperature, where the noble metals exhibit as catalysts for dissociation of gas molecules into more reactive species, thereby enhancing the gas sensitivity [34,35]. Recent researches have shown that introduction of Ag nanoparticles (AgNPs) into the MWCNTs/SnO_2 hybrids could enhance the NO_2 sensing performances at room temperature, which is attributed to the "electronic sensitization" mechanism [36]. Furthermore, the introduction of Ag NPs into the sensing materials for detecting NO_2 could also increase electronic conductivity and catalytic activity, which are other important factors for improvement of sensing performances [37,38].

In this paper, we focused on the fabrication of a novel NO_2 sensor based on AgNPs-SnO_2 nanoparticles-rGO (AgNPs-SnO_2-rGO) hybrids, where the enhancing sensing performances toward NO_2 detection at room temperature is observed by introduction of Ag NPs into SnO_2-rGO hybrids. The gas sensing performances have been examined in detailed and the results indicate that the NO_2 sensors based on AgNPs-SnO_2-rGO exhibit better sensing performances than that of SnO_2-rGO hybrids in the absence of Ag NPs.

2. Experimental

2.1. Materials

$SnCl_4{\cdot}5H_2O$, $KMnO_4$, H_2O_2 (30 wt%), $NaNO_3$, H_2SO_4 (98%), $AgNO_3$ and sodium citrate were purchased from Beijing Chemical Corp (Beijing, China). Graphite powder was purchased from Aladdin Ltd. (Shanghai, China). All chemicals were used without any further purification. The water used throughout all experiments was purified through a Millipore system.

2.2. Preparation of SnO_2-rGO hybrids

GO was prepared from natural graphite powder by a modified Hummers' method [39]. The SnO_2-rGO hybrids were prepared according to our previously reported publication [32].

2.3. Preparation of AgNPs-SnO_2-rGO hybrids

The AgNPs-SnO_2-rGO hybrids were prepared by deposition of Ag NPs on the surface of SnO_2-rGO hybrids using sodium citrate as reducing agent. In a typical run, 16 μL of 0.5 M $AgNO_3$ aqueous solution and 10 mL of 1% sodium citrate solution were introduced into 1 mL of SnO_2-rGO aqueous dispersion. The resulting mixture was heated to 100 °C and kept at this temperature for 1 h. Finally, the products were collected by centrifugation and washing several times with water for the purpose of the removal of impurities. The resulting precipitates were dispersed in water for characterization and further use.

2.4. Fabrication of gas sensors

The sensing performances of the sensors were carried out on microstructure electrodes, and a scheme to illustrate the structure of the sensor was shown in Fig. 1a. Fig. 1b shows the photographs of the signal electrode and heating electrode, respectively. The sensors were obtained by drop-coating method by dropping the aqueous dispersion of sensing materials onto the ceramic substrate coated with two pairs of Au electrodes. The photograph of a single gas sensor constructed in this work is shown in Fig. 1c.

The gas sensing properties of sensors were measured using a CGS-8 intelligent test meter (Beijing Elite Tech. Co., Ltd., China). Saturated target vapor was injected into a test chamber (about 1 L in volume) by a microinjector through a rubber plug. The gas sensing

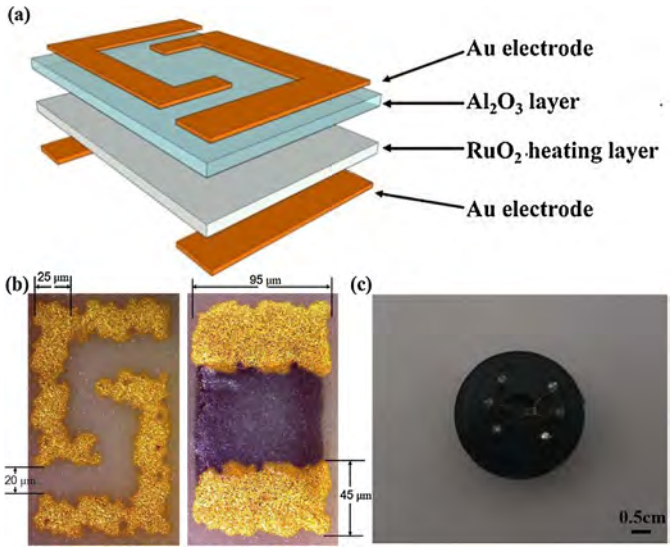

Fig. 1. (a) A schematic illustration of the NO_2 sensor, (b) the photographs of the electrodes on NO_2 sensors, (c) the photographs of the sensors coated with the sensing material.

properties of the samples were determined under specific conditions (relative humidity was about 25%). The response of a sensor was defined as the ratio (response: $S = R_a/R_g$) of the sensor resistance in air (R_a) to that in the target gas (R_g). The time taken by the sensor to achieve 90% of the total resistance change was defined as the response time in the case of adsorption and recovery time in the case of desorption.

2.5. Characterizations

Powder X-ray diffraction (XRD) data were recorded on a RigakuD/MAX 2550 diffractometer with Cu Kα radiation (λ = 1.5418 Å). UV–vis spectra were obtained on a UV-2450 Spectrophotometer. Transmission electron microscopy (TEM) measurement was made on a HITACHI H-8100 electron microscopy (Hitachi, Tokyo, Japan) with an accelerating voltage of 200 kV. The morphology of the samples was observed by field emission scanning electron microscopy (FE-SEM) on a JSM-6700F electron microscope (JEOL, Japan). Field emission scanning electron microscope (FE-SEM) equipped with an energy-dispersive X-ray spectrometer (EDX) was performed on a XL 30 ESEM FEG. X-ray photoelectron spectroscopy (XPS) analysis was measured on an ESCALABMK II X-ray photoelectron spectrometer using Mg as the exciting source. Raman spectra were obtained on J-YT64000 Raman spectrometer with 514.5 nm wavelength incident laser light.

3. Results and discussion

Fig. 2 shows the UV–vis absorption spectra of aqueous dispersion of GO, SnO_2-rGO hybrids and AgNPs-SnO_2-rGO hybrids, respectively. The UV–vis spectrum of the GO exhibits two characteristic bands at 230 nm and 305 nm, which are attributed to the electronic π–π^* transitions of C—C aromatic bonds, and the n–π^* transitions of C=O bonds [40]. It is seen that SnO_2-rGO hybrids show a broad absorption peak between 250 nm and 300 nm, after hydrothermal treatment of GO and $SnCl_4$, which is attributed to the strong absorption of SnO_2 nanoparticles [41]. Furthermore, a strong absorption band at 408 m is observed on AgNPs-SnO_2-rGO hybrids, which is attributed to the surface plasmon of AgNPs, indicating the formation of AgNPs [42]. Additionally, a band at 260 nm is also observed on AgNPs-SnO_2-rGO hybrids, which is associated with the rGO obtained by reduction of GO [42]. All these

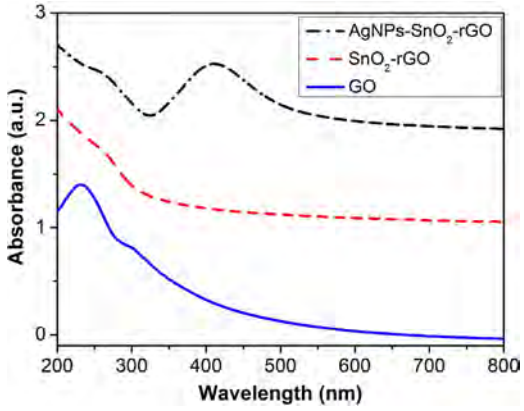

Fig. 2. UV–vis absorption spectra of aqueous dispersion of GO (blue line), SnO_2-rGO hybrids (red line) and AgNPs-SnO_2-rGO hybrids (black line). (For interpretation of the references to color in this figure legend, the reader is referred to the web version of this article.)

observations indicate that AgNPs-SnO_2-rGO hybrids have been successfully prepared by the two-step method in this work.

The structure of the AgNPs-SnO_2-rGO hybrids was further examined by the XRD technique. Fig. 3a shows the XRD patterns of GO, SnO_2-rGO hybrids and AgNPs-SnO_2-rGO hybrids, respectively. It is seen that GO exhibits a strong diffraction peak at 2θ of 10.68° attributed to (0 0 2) diffraction of GO, indicating the formation of GO by Hummers' method from graphite powder [40]. The XRD pattern of SnO_2-rGO hybrids shows four highly broadened peaks at 2θ of 26.46°, 33.48°, 51.54° and 65.40°, which are attributed to the (1 0 0), (1 0 1), (2 1 1) and (1 1 2) planes of tetragonal rutile SnO_2, indicating the formation of SnO_2 crystals, which is the same to our previous report on preparation of SnO_2-rGO hybrids [32]. It is also found that the peaks attributed to SnO_2 are also observed for AgNPs-SnO_2-rGO hybrids, indicating the presence of SnO_2. Furthermore, compared to XRD pattern of SnO_2-rGO hybrids, four diffraction peaks at 2θ of 38.22°, 44.38°, 64.52° and 77.48° are observed for the AgNPs-SnO_2-rGO hybrids, which are indexed as (1 1 1), (2 0 0), (2 2 0) and (3 1 1) diffractions of face-centered cubic crystal of Ag [43]. These observations further indicate the successful preparation of AgNPs-SnO_2-rGO hybrids.

It is well known that XPS measurement has been proven as an effective technique to examine elemental composition and chemical status for functional materials, especially for rGO-based materials. Thus, the AgNPs-SnO_2-rGO hybrids were characterized by XPS technique. Fig. 3b shows the Sn3d spectrum of AgNPs-SnO_2-rGO hybrids. It is seen that two strong peaks at 487.3 and 495.75 eV are observed, which are attributed to binding energy of $Sn3d_{3/2}$ and $Sn3d_{5/2}$, respectively, indicating the formation of SnO_2 [32]. Fig. 3c shows the Ag3d spectrum of AgNPs-SnO_2-rGO hybrids. It is well known that metallic Ag3d peaks are centered at 373.9 and 367.9 eV [44] and Ag^+ exhibits two peaks at 375.8 and 369.6 eV [45]. In the present work, AgNPs-SnO_2-rGO hybrids show the Ag3d peaks at 374.5 and 368.5 eV, suggesting that there are both metallic Ag and Ag^+ adsorbed on the AgNPs-SnO_2-rGO hybrids [46]. Based on the Ag3d XPS spectra, the content of Ag^+ in the hybrids is relatively low, and the formation of Ag^+ could be associated with the oxidation of Ag metal in air. Furthermore, it has been proven that the C1s XPS spectrum is an effective method to estimate the reduction level for chemical reduction of GO. C1s spectrum of AgNPs-SnO_2-rGO hybrids (Fig. 3d) exhibits three peaks at 284.8, 286.5 and 288.4 eV, attributed to the C—C, C—O and C=O bands in rGO-based materials [47]. Compare to the high intensity of oxygen-containing groups such as C—O, and C=O bands (data now shown), the intensity of C—C band is much higher than that of oxygen-containing groups, indicating the successful reduction

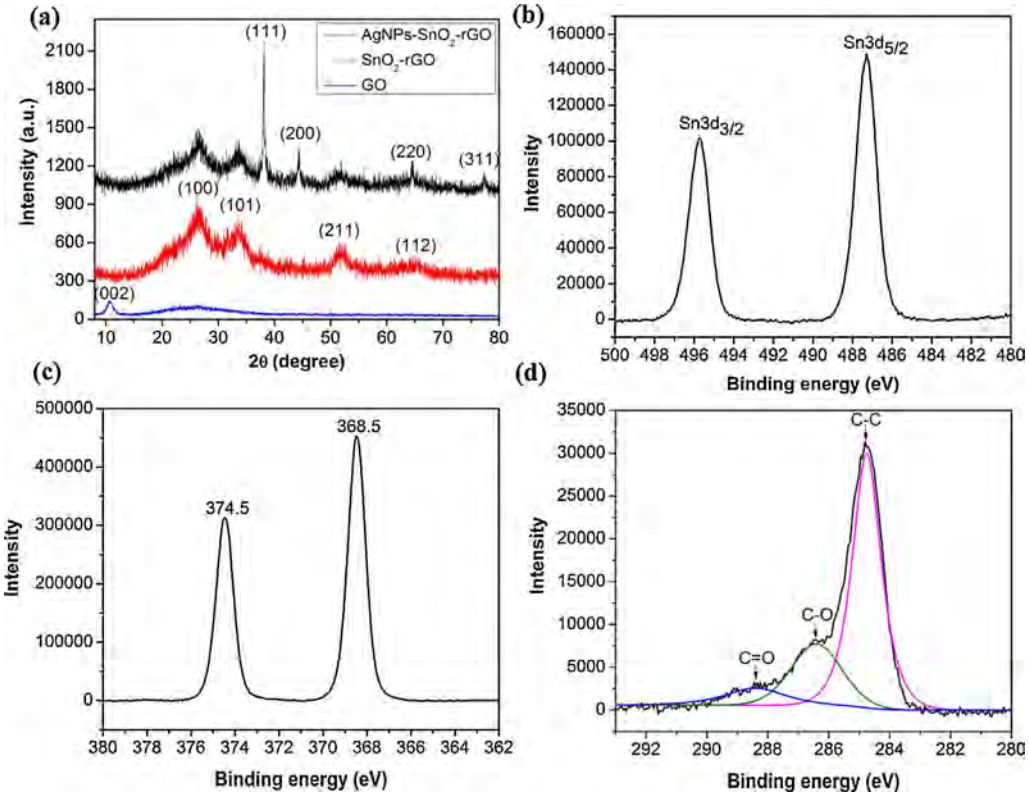

Fig. 3. (a) XRD patterns of GO (blue line), SnO_2-rGO hybrids (red line) and AgNPs-SnO_2-rGO hybrids (black line), (b) Sn3d XPS spectrum, (c) Ag3d XPS spectrum and (d) C1s XPS spectrum of AgNPs-SnO_2-rGO hybrids. (For interpretation of the references to color in this figure legend, the reader is referred to the web version of this article.)

of GO by the hydrothermal synthesis process. All these observations indicate the successful formation of SnO_2 and reduction of GO by hydrothermal treatment process and deposition of Ag NPs on SnO_2-rGO hybrids.

Fig. 4a shows the TEM image of AgNPs-SnO_2-rGO hybrids. It is seen that the hybrids exhibit typical plat morphology attributed to the presence of rGO. Compared to pure rGO, the hybrids consist of numerous nanoparticles on the surface of rGO, indicating the formation of SnO_2 nanoparticles on the rGO, further confirmed by corresponding higher magnification TEM image (Fig. 4b). Fig. 4c shows the high magnification TEM image of AgNPs-SnO_2-rGO hybrids, revealing two kinds of nanoparticles with different particle size are observed on rGO, which is different from our previously reported SnO_2-rGO hybrids [32]. The high resolution TEM (HR-TEM) image of AgNPs-SnO_2-rGO hybrids is also examined to illustrate the structure of the nanoparticles, as shown in Fig. 4d. The large size nanoparticle exhibits the lattice fringes with interplanar spacing of 0.235 nm corresponding to the (1 1 1) planes of Ag, indicating the formation of AgNPs, while the small size nanoparticle shows lattice distance of 0.33 nm ascribed to the (1 1 0) plane of SnO_2, indicating the preparation of SnO_2 nanoparticles. Based on the HR-TEM results, the particle sizes of AgNPs and SnO_2 nanoparticles are 12–15 nm and 4–5 nm, respectively. All these results further support the synthesis of AgNPs-SnO_2-rGO hybrids.

Fig. 5 shows the elemental compositions of the as-synthesized AgNPs-SnO_2-rGO hybrids investigated by EDX and elemental mapping. The presence of various well-defined peaks of C, O, Ag and Sn confirms the formation of high purity AgNPs-SnO_2-rGO hybrids. To confirm the distribution of C, O, Ag and Sn onto the lattice surface, elemental mapping of the area was carried out as shown in Fig. 5a and b and the results are depicted in Fig. 5c–f. The analysis shows that C, O, Ag and Sn are distributed homogeneously over the whole material, which further confirms the formation of AgNPs-SnO_2-rGO hybrids. Based on the results of EDX, the composition of AgNPs-SnO_2-rGO hybrids is Ag 4.80%, C 20.75%, O 28.07% and Sn 46.37%.

It is well known that Raman spectroscopy is an efficient technique to investigate the structure of rGO-based materials, and thus the structure of rGO-based materials thus obtained was further characterized by Raman spectroscopy. Fig. 6 shows Raman spectra of GO, SnO_2-rGO hybrids and AgNPs-SnO_2-rGO hybrids, respectively. It is reported that rGO-based materials exhibit a D band at about 1356 cm^{-1} and a G band at about 1600 cm^{-1}, which are attributed to a breathing mode of k-point photons of A_{1g} symmetry and the first order scattering of the E_{2g} phonon of sp^2 C atoms, respectively [48]. Although all the samples exhibit D band and G band, there are some obvious differences. Firstly, the intensities of D band to G band (I_D/I_G) of AgNPs-SnO_2-rGO hybrids (0.92) and SnO_2-rGO hybrids (0.93) are higher than that of GO (0.84), where I_D/I_G is involved in the π-conjunction extent and concentration of defects. The increasing intensity of I_D/I_G indicates the successful reduction of GO by hydrothermal treatment of GO [49]. Additionally, the increase of I_D/I_G could be attributed to the decrease in the sp^2 carbon domain and a high concentration of defects caused by an increase in vacancies, grain boundaries, amorphous carbon species, as well as SnO_2 nanoparticles inserted between rGO sheets [31]. The increased I_D/I_G intensity ratio AgNPs-SnO_2-rGO hybrids may be related to an increase in the degree of disorder of the GO matrix, in part due to chemical bonds between the carbon matrix and AgNPs [50]. Secondly, the G band of the SnO_2-rGO hybrids (1623 cm^{-1}) shows an obvious red-shift compared to that of GO (1614 cm^{-1}), which indicates the p-type doping effect between SnO_2 nanoparticles and rGO nanosheets. The p-type doping effect of SnO_2-rGO reveals the electronic interaction between SnO_2 nanoparticles and rGO nanosheets to construct a three-dimensional electron network [51]. Finally, enhanced Raman bands were observed for AgNPs-SnO_2-rGO hybrids compared to the other samples, which is attributed to the surface-enhanced Raman

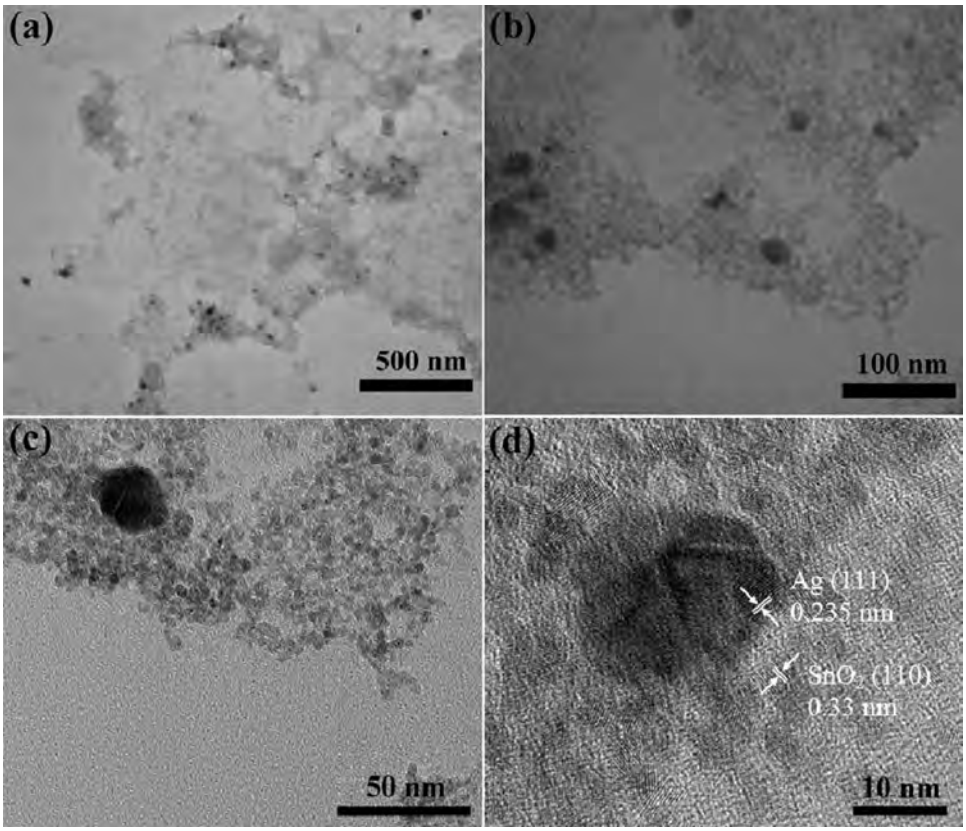

Fig. 4. (a, b) Low magnification, (c) high magnification, and (d) HR-TEM images of AgNPs-SnO_2-rGO hybrids.

scattering activity of AgNPs by electromagnetic and charge transfer mechanisms [50].

In this work, two-step wet-chemical synthesis method has been developed to prepare AgNPs-SnO_2-rGO hybrids. Firstly, a hydrothermal synthesis process is performed by heating the aqueous solution containing GO and $SnCl_4$ in an autoclave at 180 °C for 12 h. During the hydrothermal process, two reactions were carried out: (i) GO was reduced into rGO, which has been reported by the other researchers [52]. (ii) $SnCl_4$ was conversed into SnO_2 nanoparticles along with production of HCl, which has been used for preparation of SnO_2 nanoparticles [53]. As we have known, GO is also a good support for depositing inorganic nanoparticles, and thus SnO_2-rGO hybrids are obtained by this hydrothermal process. Secondly, in situ reduction method was used for preparation of AgNPs-SnO_2-rGO hybrids. It is well known that sodium citrate is an effective reducing agent for preparation of AgNPs by reduction of $AgNO_3$ under heating condition [54]. Furthermore, SnO_2-rGO hybrids are also an excellent substrate for preparation of rGO-based materials. Thus, AgNPs-SnO_2-rGO hybrids are successfully prepared by reduction of $AgNO_3$ in the presence of SnO_2-rGO hybrids. The schematic illustration for the synthesis of AgNPs-SnO_2-rGO hybrids is shown in Scheme 1.

To demonstrate the sensing application of SnO_2-rGO hybrids and AgNPs-SnO_2-rGO hybrids, NO_2 sensors were fabricated by dropping the dispersion onto the electrode as shown in Fig. 1. Fig. 7 shows the response and recovery curves to 5 ppm NO_2 of the sensor based on AgNPs-SnO_2-rGO hybrids and SnO_2-rGO hybrids at room temperature. It is seen that the response of the sensor based on AgNPs-SnO_2-rGO hybrids is 2.17, which is higher than that of SnO_2-rGO hybrids (1.31), indicating the enhancing sensing response by introduction of AgNPs. The response time and recovery time of the sensor based on AgNPs-SnO_2-rGO hybrids are 49 s and 339 s, respectively, which are shorter than that of SnO_2-rGO hybrids (415 s and 740 s). All these observations indicate that the sensing performances of the SnO_2-rGO sensor have been strongly enhanced by addition of AgNPs, which may be attributed enhancing more active sites for the adsorption of gaseous molecules and tuning the surface of rGO matrix composites group and semiconductor performance, further improving the sensing properties of rGO-based NO_2 gas sensor.

To examine the effect of the thickness for sensing materials on sensing performance, three sensors with different thicknesses (0.16, 0.49 and 1.02 μm) were fabricated and their NO_2 sensing performances were researched. The thickness of the sensing layer on the response of the gas sensor to NO_2 gas is also examined and shown in Fig. S1. It is seen that the sensor with a thickness of 0.49 μm shows the highest response (2.17), which was used for further investigation.

Fig. 8a shows the responses of the AgNPs-SnO_2-rGO hybrids operated at room temperature versus concentrations of NO_2. It is seen that the responses rapidly increase with increasing the concentrations of NO_2 from 1 to 100 ppm. The responses increase more slowly with increasing the concentrations ranging from 100 to 500 ppm, indicating that the adsorption of NO_2 by AgNPs-SnO_2-rGO hybrids has almost reached the saturation. Fig. 8b shows the response and recovery curve of the sensor based on AgNPs-SnO_2-rGO hybrids to various NO_2 concentrations ranging from 1 to 10 ppm, where the responses are 1.26, 1.70, 2.17 and 2.65, respectively, indicating that the NO_2 sensor thus constructed can be used detection of NO_2 with a wide concentration ranges. A linear fitting curve of the sensor response versus the NO_2 concentration in the range of 1–10 ppm is exhibited in Fig. S2 where the correlation coefficient R^2 of the fitting curve is 0.87. Fig. 8c shows the reproducibility of temporal response of AgNPs-SnO_2-rGO hybrids exposed to 5 ppm NO_2 at room temperature. It is seen that the sensors maintain its initial response amplitude upon three successive

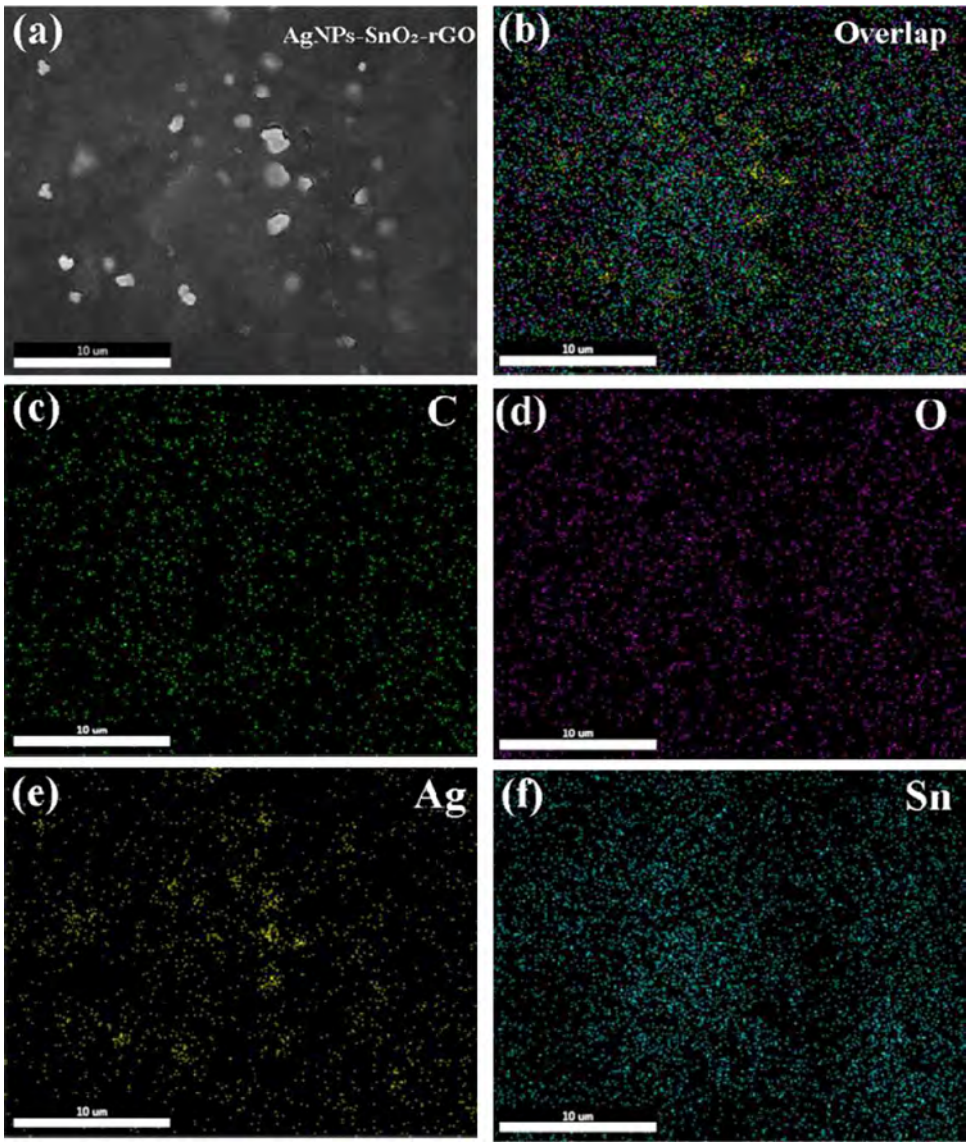

Fig. 5. The typical EDX spectrum and elemental mapping of the AgNPs-SnO_2-rGO hybrid.

sensing tests to 5 ppm NO_2, indicating that the AgNPs-SnO_2-rGO hybrids possess good repeatability. All these observations indicate that AgNPs-SnO_2-rGO hybrids are good candidate for development of high performance NO_2 sensor operating at room temperature.

Furthermore, the stability of the sensor for detection of NO_2 is also examined. Fig. S3a shows response of the AgNPs-SnO_2-rGO-based sensor to 5 ppm NO_2 for successive 15 day. It is seen that the response of the fabricated AgNPs-SnO_2-rGO-based sensor floats slightly within 5% of its initial value after 15 day. The response and recovery curve of the sensor based on AgNPs-SnO_2-rGO hybrids to 5 ppm NO_2 in the 15th day is shown in Fig. S3b revealing no obvious change of sensing properties, compared to the sensor test in the 1st day (Fig. 7a) The observed results reveal that AgNPs-SnO_2-rGO-based sensor exhibits good stability, which is very important for practical applications.

Scheme 1. Schematic illustration of the synthesis of AgNPs-SnO_2-rGO hybrids.

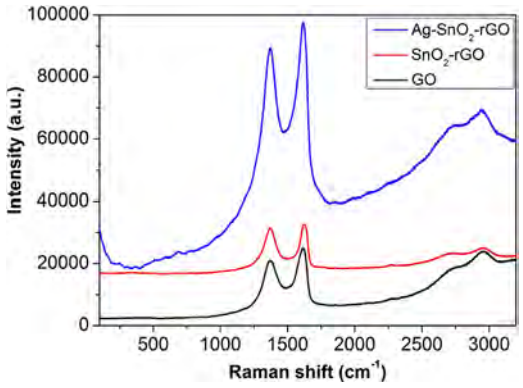

Fig. 6. (a, b) Raman spectra of GO (black line), SnO_2-rGO hybrids (red line) and AgNPs-SnO_2-rGO hybrids (blue line). (For interpretation of the references to color in this figure legend, the reader is referred to the web version of this article.)

The selectivity of the sensor based on AgNPs-SnO_2-rGO hybrids toward NO_2 is also examined. Fig. 8d shows the response of AgNPs-SnO_2-rGO hybrids at room temperature to 5 ppm of various gases, including NO_2, NO, Cl_2, NH_3, and C_2H_2. It is seen that the response of the sensor to NO_2 is much higher than that of other gases. This is because NO_2 molecule tends to interact with the active sites on rGO through its electron-deficient N atom, which enhances the electron-withdrawing ability of the oxygen functional groups [55]. In addition, the introduction of AgNPs into the SnO_2-rGO hybrids for detecting NO_2 could also increase electronic conductivity and catalytic activity, which are important factors for improvement of the sensitivity. Although Ag is also a good catalyst for C_2H_2, the AgNPs-SnO_2-rGO hybrids exhibit poor response to C_2H_2, which may be attributed the low operating temperature in the present work. Additionally, the effect of relative humidity (RH) on the sensing performance is also examined. As shown in Fig. 8d by increasing the relative humidity from 22%RH to 95%RH, no obvious response is observed, indicating the good anti-interference of AgNPs-SnO_2-rGO hybrids toward water molecules. It is well known that both NO_2 and H_2O are strong electron acceptors, which could enhance the concentration of hole in rGO after adsorbed by rGO, resulting in decreasing the resistance for gas sensing. However, the unmatching adsorption energy between H_2O and rGO results in poor response of rGO-based sensors to H_2O [56]. Furthermore, based on the theoretical calculation and the experimental data, the rGO-based gas sensors exhibit excellent selectivity toward NO_2 gas. This phenomenon is attributed to the suitable adsorption energy between NO_2 molecule and rGO materials. All these observations indicate that AgNPs-SnO_2-rGO hybrids exhibit high selectivity for NO_2 sensing.

Furthermore, the effect of annealing temperature on the sensing performances is also examined. Fig. S4 shows the response and recovery curve of the sensor based on AgNPs-SnO_2-rGO hybrids to 5 ppm NO_2 after annealing at 400 °C for 2 h. Although a obvious response to NO_2 is also observed after annealing, poor sensing performances are observed, compared to the hybrids without annealing. For instance, the sensor shows low response (1.92), long response time (324 s) and recovery time (1442 s). This may be attributed to the loss of surface area by annealing, leading to decreasing the rate for absorption and desorption of NO_2 gas. Furthermore, the effect of operating temperature on the sensing performances is also examined. Fig. S5 shows the response and recovery curves of the sensor based on AgNPs-SnO_2-rGO hybrids to 5 ppm NO_2 operating at various temperatures ranging from 30 to 70 °C. It is seen that the responses decrease with increasing the operating temperature, which is similar with our previous report [32]. Additionally, the response time and recovery time also decrease with increasing the operating temperature.

Furthermore, the effect of annealing temperature on the sensing performances is also examined. Fig. S4 shows the response and recovery curve of the sensor based on AgNPs-SnO_2-rGO hybrids to 5 ppm NO_2 after annealing at 400 °C for 2 h. Although an obvious response to NO_2 is also observed after annealing, poor sensing performances are observed, compared to the hybrids without annealing. For instance, the sensor shows low response (1.92), long response time (324 s) and recovery time (1442 s). This may be attributed to the loss of surface area by annealing, leading to decreasing the rate for absorption and desorption of NO_2 gas. Furthermore, the effect of operating temperature on the sensing performances is also examined. Fig. S5 shows the response and recovery curves of the sensor based on AgNPs-SnO_2-rGO hybrids to 5 ppm NO_2 operating at various temperatures ranging from 30 to 70 °C. It is seen that the responses decrease with increasing the operating temperature, which is similar with our previous report [32]. Additionally, the response time and recovery time also decrease with increasing the operating temperature.

It is well known that the gas sensing performances of rGO materials can be enhanced by modification with metal oxide nanoparticles. The sensing performances of the NO_2 sensor based on AgNPs-SnO_2-rGO hybrids were also compared with the previously reported NO_2 sensors based on rGO-based materials, as shown in Table 1. The response of AgNPs-SnO_2-rGO hybrids to NO_2 is higher than that of Cu_2O-rGO [22] and In_2O_3-rGO [57]. Although the response of AgNPs-SnO_2-rGO hybrids to NO_2 is lower than that of WO_3-rGO [20] and Co_3O_4-rGO [21] at room temperature, the sensor in this work exhibits shorter response time and recovery time. Furthermore, the sensing performances of the sensor based on AgNPs-SnO_2-rGO hybrids are also compared with pure SnO_2-based NO_2 sensors. Most of the SnO_2-based NO_2 sensors are operated at

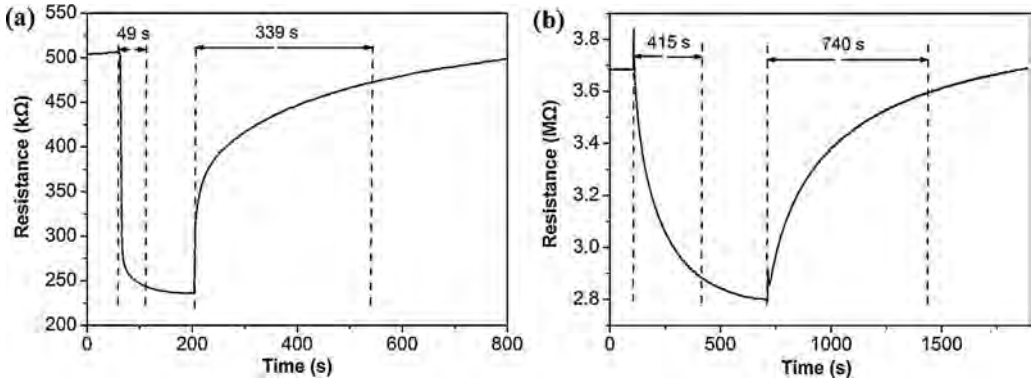

Fig. 7. (a) The response recovery curves to 5 ppm NO_2 of the sensor based on (b) SnO_2-rGO hybrids and (c) AgNPs-SnO_2-rGO hybrids at room temperature.

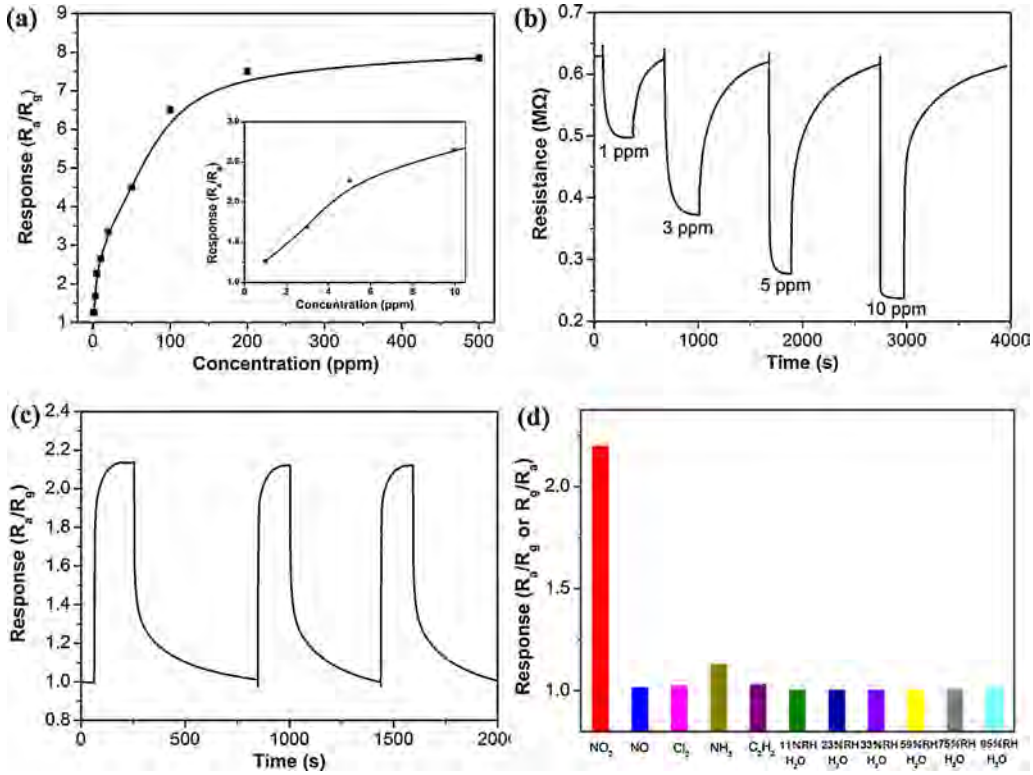

Fig. 8. (a) The responses of AgNPs-SnO_2-rGO-based sensor to different concentrations of NO_2 at room temperature, (b) response and recovery curve of the sensor based on AgNPs-SnO_2-rGO hybrids to various NO_2 concentrations of 1 ppm, 3 ppm, 5 ppm, 10 ppm at room temperature, (c) The reproducibility of temporal response of AgNPs-SnO_2-rGO hybrids exposed to 5 ppm NO_2 at room temperature, and (d) the selectivity of the sensors based on AgNPs-SnO_2-rGO hybrids toward 5 ppm gases, including NO_2, NO, Cl_2, NH_3, C_2H_2 and H_2O (different relative humidity) at room temperature.

high operating temperature [9], and thus the huge advantage of the AgNPs-SnO_2-rGO hybrids-based NO_2 sensor is low operating temperature. To satisfy the practical applications for detection of NO_2 operating at room temperature, additional work is also required to further enhance the sensing performances of NO_2 sensor based on AgNPs-SnO_2-rGO hybrids. For example, the sensor in this work exhibits shorter response time and recovery time at room temperature, compared to the previously reported rGO-based sensors. It is well known that the recovery time is related to the intimate chemical interactions between the sensing materials and adsorbed gas molecules [58]. For rGO-based sensors, and the recovery time can be shorten by heating the sensors at high temperature [18] or irradiation the sensors by the UV light [59]. In addition to the possible damage to the rGO film structure, irradiation and heating treatments are time- and energy consuming, which contributes to increased associated costs. Another possible technique to decrease the recovery time is chemical doping of boron or nitrogen in rGO. Insertion of such heteroatom (such as N, and B) could tune the electronic properties of rGO. Meanwhile, the physical and chemical properties of rGO are also altered by the introduction of doped atoms, which could be extremely useful for enhancing the performance of gas sensors [60]. Indeed, Niu et al. have reported that the response time and recovery time of the sensor based on N and Si co-doped graphene for 21 ppm NO_2 are 68 s and 635 s, where the short recovery time is attributed to the introduction of doped atoms [61].

The sensing mechanism of the sensor based on AgNPs-SnO_2-rGO hybrids toward the detection of NO_2 is also discussed. First of all, the most important factor for good sensing performances is the presence of rGO. The superior electrical properties of rGO, such as high carrier mobility at room temperature, and detectable change in their resistance after adsorption or desorption of guest gases, contribute to application of AgNPs-SnO_2-rGO hybrids for NO_2 sensing at room temperature.

The improvement of sensing performances, especially compared to SnO_2-rGO hybrids, is attributed to the tuning the structure of sensing materials by introduction of AgNPs into SnO_2-rGO hybrids and the possible reasons for enhancing sensing performances may be proposed as follows: (i) the introduction of AgNPs increases the electron transfer rate of sensing materials. As shown in Fig. 9, the AgNPs-SnO_2-rGO hybrids exhibit much larger slope than that of SnO_2-rGO hybrids, indicating the low resistance of AgNPs-SnO_2-rGO hybrids, which is also confirmed by response and recovery curve shown in Fig. 7, (ii) the introduction of AgNPs also effects the porous structure of sensing materials. Fig. S6 shows N_2 sorption isothermals and pore size distribution curves of

Table 1
Comparison of sensing performances of our proposed NO_2 sensor with other published NO_2 sensors based on metal oxide-rGO hybrids at room temperature.

Materials	Concentration (ppm)	Operating temperature (°C)	Response	Response time and recovery time (s/s)	Ref.
WO_3-rGO	5	RT	769%	540 s/1080 s	[20]
Co_3O_4-rGO	60	RT	80%	–/no recovery	[21]
Cu_2O-rGO	2	RT	67.8%	–/–	[22]
In_2O_3-rGO	5	RT	37.81%	–/–	[57]
AgNPs-SnO_2-rGO	5	RT	2.17	49 s/339 s	This work

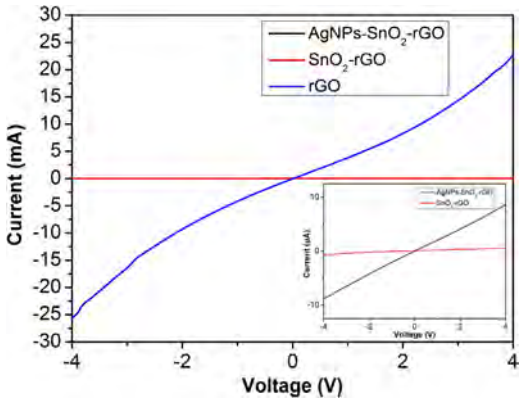

Fig. 9. Representative *I–V* curves for rGO (blue line), SnO_2-rGO (red line) and AgNPs-SnO_2-rGO (black line). (For interpretation of the references to color in this figure legend, the reader is referred to the web version of this article.)

SnO_2-rGO hybrids and AgNPs-SnO_2-rGO hybrids. The BET surface area of SnO_2-rGO hybrids is 212 m^2/g, which is higher than that of Ag-SnO_2-rGO hybrids (91 m^2/g). Notably, the pore size of AgNPs-SnO_2-rGO hybrids is 3.2 nm, which is larger than of SnO_2-rGO hybrids (2.1 nm). The relatively large pore size could increase the adsorption and desorption rate of NO_2 molecules, which may be another factor for enhanced the sensing performances of AgNPs-SnO_2-rGO hybrids. (iii) The introduction of AgNPs leadings to formation of new heterojunctions between the various components in sensing materials. In the case of SnO_2-rGO hybrids, p-n heterojunction is formed between n-type SnO_2 and p-type rGO, which could increase the electron transfer rate during the detection process. In the case of AgNPs-SnO_2-rGO hybrids, the introduction of AgNPs, a typical noble metal, could result in formation of nano-Sttocky contact between Ag metal and the p-type rGO or n-type SnO_2. (iv) The enhanced sensing performances obtained by the "electronic mechanism" and "chemical mechanism" due to the introduction of AgNPs. The "electronic mechanism" proposes the formation of depletion zones around the SnO_2 particles by addition of AgNPs attributed to the modulation of the nano-Schottky barriers, thereby improving the surface reactivity at low temperature. An alternative "chemical mechanism" proposes that the AgNPs activate and dissociate of molecular oxygen, whose atomic products then diffuse to the SnO_2 support by the spill-over effect. This process greatly increases both the quantity of oxygen that can repopulate vacancies on the SnO_2 surface and the rate at which this repopulation occurs, resulting in a greater (and faster) degree of electron withdrawal from the SnO_2 at lower temperature [36]. (v) The catalytic activity of AgNPs could also enhance the gas sensing performances. AgNPs could tailor the surface active sites over the surface SnO_2-rGO hybrids, which could enhance the adsorption and desorption of NO_2 gas owing to the high catalytic or conductive nature of Ag [62].

The sensing process of AgNPs-SnO_2-rGO-based sensor for NO_2 is possibly proposed as follow. In this work, the components of the hybrids are comprised of p-type rGO, n-type SnO_2 and noble metal Ag. When AgNPs-SnO_2-rGO hybrids are exposed to air, the oxygen molecules are adsorbed on their surface and electrons captured from the conduction band of SnO_2 nanoparticles to form the first depletion layer (O^{2-}, O_2^- or O^-). The second depletion layer is formed by p-n junction at the interface of n-type SnO_2 and p-type rGO in the hybrids. The modulation of resistance of the sensors by formation of p-n junction between n-type SnO_2 and p-type rGO is another important factor for enhancing the sensitivity for NO_2 sensing. In fact, the experimental observation of the conductivity decrease of the rGO sensor after SnO_2 nanoparticles decoration suggests the formation of a hole depletion layer of the p-type rGO near the interface with n-type SnO_2. In addition, the introduction of AgNPs could result in formation of nano-Sttocky contact between AgNPs and p-type rGO or n-type SnO_2. The AgNPs can dissociate and chemisorb O_2 under atmospheric conditions. Thus, electron depletion zones form around AgNPs by oxygen adsorption. The work function of these regions is higher than that of SnO_2 nanoparticles [36], which result in the forming nano-Schottky barriers at the Ag-SnO_2 interface, leading to an electron transfer from SnO_2 and rGO to AgNPs.

It should be noted that the formation of p-n junction between SnO_2 and rGO plays an important role in improving the sensing performance for rGO-based sensors. Scheme 2 shows a scheme to illustrate the mechanism for formation of p-n junction of SnO_2-rGO hybrids. As reported in the previous publication, since work functions of n-type SnO_2 and p-type rGO are about 4.55 and 4.75 eV, thus electrons will flow from SnO_2 to rGO, establishing the hole-depletion region [28]. This phenomenon is also the similar with the sensors based on MWCNTs/SnO_2 hybrids [63]. The sensing mechanism for NO_2 sensing based on SnO_2-rGO hybrids could be described as follows: When the sensor based on SnO_2-rGO hybrids is exposed to NO_2, the gas molecules could attract the electrons from SnO_2-rGO hybrids, which leads to electron transfer from the SnO_2-rGO hybrids to surface adsorbates NO_2. The adsorption of NO_2 on SnO_2-rGO hybrids leads to NO_2^-. The process induces electrons flow from SnO_2 to rGO, leading to the increasing hole density. It finally results in a rapid decrease of the resistance and higher sensitivity. Moreover, NO_2 directly adsorbs onto SnO_2-rGO hybrids and react with O_2^- (the stable oxygen ions are O_2^- below 100 °C [64]) and generate NO_3^- [55]. It is well known that the effects of the p-n heterojunctions between SnO_2 and rGO would play an important role, but the attachment of SnO_2 nanoparticles onto the rGOs also leads to more active sites (such as defect sites and functional groups) for the absorption of NO_2 molecules.

In this work, the experimental data indicate that AgNPs-SnO_2-rGO hybrids exhibit as a typical p-type semiconductor for detection of NO_2. By putting the sensor into NO_2 atmosphere, the adsorbed oxygen (O^{2-}, O_2^- or O^-) on the SnO_2 surface will interact with NO_2 gas molecules, resulting in transferring electron from hybrids to NO_2 molecule. Thus, the concentration of hole in the hybrids increases after adsorption of NO_2, leading to decreasing the resistance of hybrids. By putting the sensor into air atmosphere for sensor recovery, the NO_2 molecules are desorbed from hybrids, along with returning the electron back to hybrids. Thus, the concentration of hole in the hybrids decreases and the resistance of the sensor increases. However, the exact sensing mechanism of AgNPs-SnO_2-rGO hybrids for detection of NO_2 is not completely understood at present time and requires further study.

Furthermore, the improvement of response and recovery rate of AgNPs-SnO_2-rGO-based sensor compared to SnO_2-rGO-based sensor may be attributed to the following reasons: (i) The relatively large pore size of AgNPs-SnO_2-rGO hybrids could increase the adsorption and desorption rate of NO_2 molecules. (ii) The introduction of AgNPs could result in formation of nano-Sttocky contact between Ag metal and the p-type rGO or n-type SnO_2. This all could increase the electron transfer rate during the detection process. (iii) AgNPs could activate and dissociate of molecular oxygen. This process greatly increases both the quantity of oxygen that can repopulate vacancies on the SnO_2 surface, resulting in a greater (and faster) degree of electron withdrawal from the SnO_2 at a lower temperature. Furthermore, this process could also increase the electron transfer rate. (iv) The catalytic activity of AgNPs could also enhance response and recovery rate of AgNPs-SnO_2-rGO hybrids. Because AgNPs could control the surface active sites over the SnO_2-rGO hybrids surface, which could enhance the adsorption and desorption of NO_2 gas owing to the high catalytic or conductive nature of Ag.

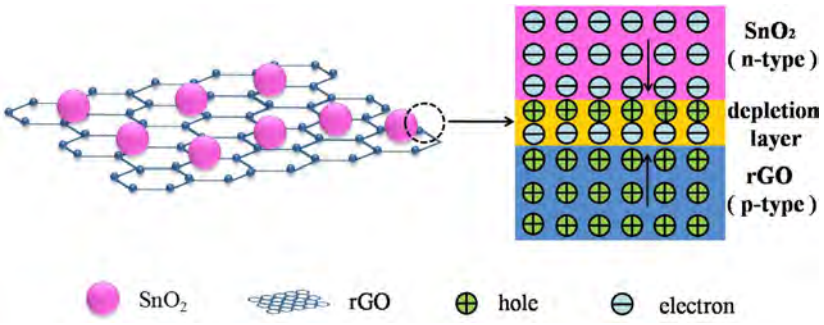

Scheme 2. A scheme to illustrate the mechanism for formation of p-n junction of SnO_2-rGO hybrids.

4. Conclusions

In summary, a new NO_2 sensor has been successfully fabricated by using AgNPs-SnO_2-rGO hybrids as sensing materials, which have been prepared by hydrothermal synthesis method. The gas sensing results indicate that the introduction of AgNPs into the SnO_2-rGO hybrids significantly enhanced the NO_2 sensing performances at room temperature, compared to SnO_2-rGO hybrids. Our present study is of importance because it provides a new sensing material for fabrication of high-performance room temperature NO_2 sensors.

Acknowledgments

This research work was financially supported by the National Natural Science Foundation of China (Grant No. 51202085), Program for Chang Jiang Scholars and Innovative Research Team in University (Grant No. IRT3018) and the Open Project from State Key Laboratory of Transducer Technology (Grant No. SKT1402).

Appendix A. Supplementary data

Supplementary data associated with this article can be found, in the online version, at http://dx.doi.org/10.1016/j.snb.2015.09.027.

References

[1] R. Atkinson, Atmospheric chemistry of VOCs and NO_x, Atmos. Environ. 34 (2000) 2063–2101.
[2] D. Zhang, Z. Liu, C. Li, T. Tang, X. Liu, S. Han, B. Lei, C. Zhou, Detection of NO_2 down to ppb levels using individual and multiple In_2O_3 nanowire devices, Nano Lett. 4 (2004) 1919–1924.
[3] N.D. Chinh, N.V. Toan, V.V. Quang, N.V. Duy, N.D. Hoa, N.V. Hieu, Comparative NO_2 gas-sensing performance of the self-heated individual, multiple and networked SnO_2 nanowire sensors fabricated by a simple process, Sens. Actuators B 201 (2014) 7–12.
[4] J.C. Yang, P.K. Dutta, Influence of solid-state reactions at the electrode–electrolyte interface on high-temperature potentiometric NO_x-gas sensors, J. Phys. Chem. C 111 (2007) 8307–8313.
[5] S.I. Ohira, P.K. Dasgupta, K.A. Schug, Fiber optic sensor for simultaneous determination of atmospheric nitrogen dioxide, ozone, and relative humidity, Anal. Chem. 81 (2009) 4183–4191.
[6] C. Wen, C. Zhu, Y. Ju, H. Xu, Y. Qiu, A novel NO_2 gas sensor using dual track SAW device, Sens. Actuators A 159 (2010) 168–173.
[7] D.S. Lee, S.D. Han, J.S. Huh, D.D. Lee, Nitrogen oxides-sensing characteristics of WO_3-based nanocrystalline thick film gas sensor, Sens. Actuators B 60 (1999) 57–63.
[8] M.W. Ahn, K.S. Park, J.H. Heo, J.G. Park, D.W. Kim, K.J. Choi, J.H. Lee, S.H. Hong, Gas sensing properties of defect-controlled ZnO-nanowire gas sensor, Appl. Phys. Lett. 93 (2008) 263103.
[9] M. Tonezzer, N.V. Hieu, Size-dependent response of single-nanowire gas sensors, Sens. Actuators B 163 (2012) 146–152.
[10] K. Soulantica, L. Erades, M. Sauvan, F. Senocq, A. Maisonnat, B. Chaudret, Synthesis of indium and indium oxide nanoparticles from indium cyclopentadienyl precursor and their application for gas sensing, Adv. Funct. Mater. 13 (2003) 553–557.
[11] A.K. Geim, K.S. Novoselov, The rise of graphene, Nat. Mater. 6 (2007) 183–191.
[12] S. Stankovich, D.A. Dikin, R.D. Piner, K.A. Kohlhaas, A. Kleinhammes, Y. Jia, Y. Wu, S.T. Nguyen, R.S. Ruoff, Synthesis of graphene-based nanosheets via chemical reduction of exfoliated graphite oxide, Carbon 45 (2007) 1558–1565.
[13] K. Ratinac, W. Yang, S.P. Ringer, F. Braet, Toward ubiquitous environmental gas sensors-capitalizing on the promise of graphene, Environ. Sci. Technol. 44 (2010) 1167–1176.
[14] F. Schedin, A.K. Geim, S.V. Morozov, E.W. Hill, P. Blake, M.I. Katsnelson, K.S. Novoselov, Detection of individual gas molecules adsorbed on graphene, Nat. Mater. 6 (2007) 652–655.
[15] Q. Lin, Y. Li, M. Yang, Tin oxide/graphene composite fabricated via a hydrothermal method for gas sensors working at room temperature, Sens. Actuators B 173 (2012) 139–147.
[16] W. Yuan, G. Shi, Graphene-based gas sensors, J. Mater. Chem. A 1 (2013) 10078–10091.
[17] T.H. Han, Y.K. Huang, A.T.L. Tan, V.P. Dravid, J. Huang, Steam etched porous graphene oxide network for chemical sensing, J. Am. Chem. Soc. 133 (2011) 15264–15267.
[18] G. Lu, S. Park, K. Yu, R.S. Ruoff, L.E. Ocola, D. Rosenmann, J. Chen, Toward practical gas sensing with highly reduced graphene oxide: a new signal processing method to circumvent run-to-run and device-to-device variations, ACS Nano 5 (2011) 1154–1164.
[19] S. Liu, B. Yu, H. Zhang, T. Fei, T. Zhang, Enhancing NO_2 gas sensing performances at room temperature based on reduced graphene oxide-ZnO nanoparticles hybrids, Sens. Actuators B 202 (2014) 272–278.
[20] P.G. Su, S.L. Peng, Fabrication and NO_2 gas-sensing properties of reduced graphene oxide/WO_3 nanocomposite films, Talanta 132 (2015) 398–405.
[21] N. Chen, X. Li, X. Wang, J. Yu, J. Wang, Z. Tang, S.A. Akbarb, Enhanced room temperature sensing of Co_3O_4-intercalated reduced graphene oxide based gas sensors, Sens. Actuators B 188 (2013) 902–908.
[22] S. Deng, V. Tjoa, H. Fan, H. Tan, D.C. Sayle, M. Olivo, S. Mhaisalkar, J. Wei, C.H. Sow, Reduced graphene oxide conjugated Cu_2O nanowire mesocrystals for high-performance NO_2 gas sensor, J. Am. Chem. Soc. 134 (2012) 4905–4917.
[23] L. Zhou, F. Shen, X. Tian, D. Wang, T. Zhang, C. Wei, Stable Cu_2O nanocrystals grown on functionalized graphene sheets and room temperature H_2S gas sensing with ultrahigh sensitivity, Nanoscale 5 (2013) 1564–1569.
[24] S. Srivastava, K. Jain, V.N. Singh, S. Singh, N. Vijayan, N. Dilawar, G. Gupta, T.D. Senguttuvan, Faster response of NO_2 sensing in graphene-WO_3 nanocomposites, Nanotechnology 23 (2012) 205501–205508.
[25] J.H. Lee, A. Katoch, S.W. Choi, J.H. Kim, H.W. Kim, S.S. Kim, Extraordinary improvement of gas-sensing performances in SnO_2 nanofibers due to creation of local p-n heterojunctions by loading reduced graphene oxide nanosheets, ACS Appl. Mater. Interfaces 7 (2015) 3101–3109.
[26] C. Marichy, P.A. Russo, M. Latino, J.P. Tessonnier, M.G. Willinger, N. Donato, G. Neri, N. Pinna, Tin dioxide-carbon heterostructures applied to gas sensing: structure-dependent properties and general sensing mechanism, J. Phys. Chem. C 117 (2013) 19729–19739.
[27] G. Neria, S.G. Leonardia, M. Latinob, N. Donatoc, S. Baekd, D.E. Contee, P.A. Russoe, N. Pinna, Sensing behavior of SnO_2/reduced graphene oxide nanocomposites toward NO_2, Sens. Actuators B 179 (2013) 61–68.
[28] S. Mao, S. Cui, G. Lu, K. Yu, Z. Wen, J. Chen, Tuning gas-sensing properties of reduced graphene oxide using tin oxide nanocrystals, J. Mater. Chem. 22 (2012) 11009–11013.
[29] S. Cui, Z. Wen, E.C. Mattson, S. Mao, J. Chang, M. Weinert, C.J. Hirschmugl, M. Gajdardziska-Josifovska, J. Chen, Indium-doped SnO_2 nanoparticle-graphene nanohybrids: simple one-pot synthesis and their selective detection of NO_2, J. Mater. Chem. A 1 (2013) 4462–4467.
[30] X. Liu, J. Cui, J. Sun, X. Zhang, 3D graphene aerogel-supported SnO_2 nanoparticles for efficient detection of NO_2, RSC Adv. 4 (2014) 22601–22605.
[31] L. Li, S. He, M. Liu, C. Zhang, W. Chen, Three-dimensional mesoporous graphene aerogel-supported SnO_2 nanocrystals for high-performance NO_2 gas sensing at low temperature, Anal. Chem. 87 (2015) 1638–1645.
[32] H. Zhang, J. Feng, T. Fei, S. Liu, T. Zhang, SnO_2 nanoparticles-reduced graphene oxide nanocomposites for NO_2 sensing at low operating temperature, Sens. Actuators B 190 (2014) 472–478.
[33] S. Liu, Z. Wang, Y. Zhang, C. Zhang, T. Zhang, High performance room temperature NO_2 sensors based on reduced graphene oxide-multiwalled carbon nanotubes-tin oxide nanoparticles hybrids, Sens. Actuators B 211 (2015) 318–324.

[34] S.W. Choi, S.H. Jung, S.S. Kim, Functionalization of selectively grown networked SnO_2 nanowires with Pd nanodots by γ-ray radiolysis, Nanotechnology 22 (2011) 225501.
[35] S.S. Kim, J.Y. Park, S.W. Choi, H.S. Kim, H.G. Na, J.C. Yang, H.W. Kim, Significant enhancement of the sensing characteristics of In_2O_3 nanowires by functionalization with Pt nanoparticles, Nanotechnology 21 (2010) 415502.
[36] S. Cui, H. Pu, E.C. Mattson, G. Lu, S. Mao, M. Weinert, C.J. Hirschmugl, M. Gajdardziska-Josifovska, J. Chen, Ag nanocrystal as a promoter for carbon nanotube-based room-temperature gas sensors, Nanoscale 4 (2012) 5887–5894.
[37] S.W. Choi, A. Katoch, G.J. Sun, P. Wu, S.S. Kim, NO_2-sensing performance of SnO_2 microrods by functionalization of Ag nanoparticles, J. Mater. Chem. C 1 (2013) 2834–2841.
[38] L. Wang, B. Han, Z. Wang, L. Dai, H. Zhou, Y. Lia, H. Wang, Effective improvement of sensing performance of amperometric NO_2 sensor by Ag-modified nano-structured CuO sensing electrode, Sens. Actuators B 207 (2015) 791–800.
[39] W.S. Hummers Jr., R. Offeman, Preparation of graphitic oxide, J. Am. Chem. Soc. 80 (1958) 1339.
[40] S. Liu, J. Tian, L. Wang, H. Li, Y. Zhang, X. Sun, Stable aqueous dispersion of graphene nanosheets: noncovalent functionalization by a polymeric reducing agent and their subsequent decoration with Ag nanoparticles for enzymeless hydrogen peroxide detection, Macromolecules 43 (2010) 10078–10083.
[41] S.K. Park, S.H. Yu, N. Pinna, S. Woo, B. Jang, Y.H. Chung, Y.H. Cho, Y.E. Sung, Y. Piao, A facile hydrazine-assisted hydrothermal method for the deposition of monodisperse SnO_2 nanoparticles onto graphene for lithium ion batteries, J. Mater. Chem. 22 (2012) 2520.
[42] J. Li, C. Liu, Ag/graphene heterostructures: synthesis, characterization and optical properties, Eur. J. Inorg. Chem. 8 (2010) 1244–1248.
[43] B. Yu, J. Feng, S. Liu, T. Zhang, Preparation of reduced graphene oxide decorated with high density Ag nanorods for non-enzymatic hydrogen peroxide detection, RSC Adv. 3 (2013) 14303–14307.
[44] V.G. Pol, D.N. Srivastava, O. Palchik, V. Palchik, M.A. Slifkin, A.M. Weiss, A. Ge-danken, Sonochemical deposition of silver nanoparticles on silica spheres, Langmuir 18 (2002) 3352–3357.
[45] X. Sun, S. Dong, E. Wang, One-step preparation and characterization of poly (propyleneimine) dendrimer-protected silver nanoclusters, Macromolecules 37 (2004) 7105–7108.
[46] J. Tian, S. Liu, X. Sun, Supramolecular microfibrils of o-phenylenediamine dimers: oxidation-induced morphology change and the spontaneous formation of Ag nanoparticle decorated nanofibers, Langmuir 26 (2010) 15112–15116.
[47] S. Pei, J. Zhao, J. Du, W. Ren, H. Cheng, Direct reduction of graphene oxide films into highly conductive and flexible graphene films by hydrohalic acids, Carbon 48 (2010) 4466–4474.
[48] X. Qin, Y. Luo, W. Lu, G. Chang, A.M. Asiri, A.O. Al-Youbi, X. Sun, One-step synthesis of Ag nanoparticles-decorated reduced graphene oxide and their application for H_2O_2 detection, Electrochim. Acta 79 (2012) 46–51.
[49] M.K. Joshi, H.R. Pant, H.J. Kimd, J.H. Kim, C.S. Kim, One-pot synthesis of Ag-iron oxide/reduced graphene oxide nanocomposite via hydrothermal treatment, Colloids Surf. A 446 (2014) 102–108.
[50] Q. Bao, D. Zhang, P. Qi, Synthesis and characterization of silver nanoparticle and graphene oxide nanosheet composites as a bactericidal agent for water disinfection, J. Colloid Interface Sci. 360 (2011) 463–470.
[51] B. Das, R. Voggu, C.S. Rout, C.N.R. Rao, Changes in the electronic structure and properties of graphene induced by molecular charge-transfer, Chem. Commun. 41 (2008) 5155–5157.
[52] Y. Zhou, Q. Bao, L. Tang, Y. Zhong, K.P. Loh, Hydrothermal dehydration for the "Green" reduction of exfoliated graphene oxide to graphene and demonstration of tunable optical limiting properties, Chem. Mater. 21 (2009) 2950–2956.
[53] Y. Du, S. Liu, Y. Ji, Y. Zhang, S. Wei, F. Liu, F.S. Xiao, Synthesis of sulfated silica-doped tin oxides and their high activities in transesterification, Catal. Lett. 124 (2008) 133–138.
[54] W. Lu, Y. Luo, G. Chang, X. Sun, Synthesis of functional SiO_2-coated graphene oxide nanosheets decorated with Ag nanoparticles for H_2O_2 and glucose detection, Biosens. Bioelectron. 26 (2011) 4791–4797.
[55] F. Gu, R. Nie, D. Han, Z. Wang, In_2O_3-graphene nanocomposite based gas sensor for selective detection of NO_2 at room temperature, Sens. Actuators B 219 (2015) 94–99.
[56] O. Leenaerts, B. Partoens, F.M. Peeters, Adsorption of H_2O, NH_3, CO, NO_2, and NO on graphene: a first-principles study, Phys, Rev. B 77 (2008) 125416.
[57] W. Yang, P. Wan, X. Zhou, J. Hu, Y. Guan, L. Feng, Additive-free synthesis of In_2O_3 cubes embedded into graphene sheets and their enhanced NO_2 sensing performance at room temperature, ACS Appl. Mater. Interfaces 6 (2014) 21093–21100.
[58] F. Perreault, A.F.D. Faria, M. Elimelech, Environmental applications of graphene-based nanomaterials, Chem. Soc. Rev. 44 (2015) 5861–5896.
[59] V. Dua, S.P. Surwade, S. Ammu, S.R. Agnihotra, S. Jain, K.E. Roberts, S. Park, R.S. Ruoff, S.K. Manohar, All-organic vapor sensor using inkjet-printed reduced graphene oxide, Angew. Chem. Int. Ed. 49 (2010) 2154–2157.
[60] S.S. Varghese, S. Lonkar, K.K. Singh, S. Swaminathan, A. Abdala, Recent advances in graphene based gas sensors, Sens. Actuators B 218 (2015) 160–183.
[61] F. Niu, J.M. Liu, L.M. Tao, W. Wang, W.G. Song, Nitrogen and silica co-doped graphene nanosheets for NO_2 gas sensing, J. Mater. Chem. A 1 (2013) 6130–6133.
[62] E.H. Espinosa, R. Ionescu, C. Bittencourt, A. Felten, R. Erni, G.V. Tendeloo, J.J. Pireaux, E. Llobet, Metal-decorated multi-wall carbon nanotubes for low temperature gas sensing, Thin Solid Films 515 (2007) 8322–8327.
[63] G. Lu, L.E. Ocola, J. Chen, Room-temperature gas sensing based on electron transfer between discrete tin oxide nanocrystals and multiwalled carbon nanotubes, Adv. Mater. 21 (2009) 2487–2491.
[64] A.S.M. Iftekhar Uddin, D.T. Phan, G.S. Chung, Low temperature acetylene gas sensor based on Ag nanoparticles-loaded ZnO-reduced graphene oxide hybrid, Sens. Actuators B 207 (2015) 362–369.

Biographies

Ziying Wang received her BS degree from the College of Electronics Science and Engineering, Jilin University, China in 2013. During BS course, she studied in Tomsk and received her BS degree from the College of Institute of Non-Destructive Testing, Tomsk Polytechnic University, Russia in 2013. She entered the MS course in 2013. Now her research focuses on preparation of gas sensors and flexible strain sensors.

Yong Zhang received his BS degree from the College of Science, Changchun University of Science and Technology, China in 2011. He received his MS degree from the College of Science, Changchun University of Science and Technology, China in 2014. During MS course, he took part in the joint training program for two years in Changchun Institute of Applied Chemistry, Chinese Academy of Sciences. He entered the DS course in 2014, majoring in microelectronics and solid-state electronics. His research focuses on the preparation of electrochemical sensor based on nano-micron functional materials.

Sen Liu received his BS degree in 2005 in Chemistry and PhD degree in 2010 in Inorganic Chemistry from Jilin University. Now he is an associate professor in Jilin University and his current research is focused on the carbon-based functional materials and chemical sensors.

Tong Zhang completed her MS degree in semiconductor materials in 1992 and her PhD degree in the field of microelectronics and solid-state electronics in 2001 from Jilin University. She was appointed as a full-time professor in the College of Electronics Science and Engineering, Jilin University in 2001. Her research interests are sensing functional materials, gas sensors, humidity sensors and electrochemical sensors.